

Numerical modelling of instability and supercritical oscillatory states in a Czochralski model system of oxide melts

N. Crnogorac^{*1}, H. Wilke¹, K. A. Cliffe², A. Yu. Gelfgat³, and E. Kit³

¹ Institute for Crystal Growth (IKZ), Max-Born-Str. 2, D-12489 Berlin, Germany

² School of Mathematical Sciences, Nottingham University, University Park, Nottingham NG7 2RD, UK

³ School of Mechanical Engineering, Faculty of Engineering, Tel-Aviv University, Israel

Received 6 March 2008, revised 31 March 2008, accepted 1 April 2008

Published online 9 May 2008

Key words computer simulation, fluid flows, heat transfer, mass transfer, Czochralski method.

PACS 81.10.Fq, 47.20.-k, 47.20.Bp, 47.20.Ky, 02.60.Cb, 02.30.Oz

The motivation for this study is the need for accurate numerical models of melt flow instabilities during Czochralski growth of oxides. Such instabilities can lead to undesirable spiralling shapes of the bulk crystals produced by the growing process. The oxide melts are characterized by Prandtl numbers in the range $5 < Pr < 20$, which makes the oxide melt flow qualitatively different from the intensively studied flows of semiconductors characterized by smaller Prandtl numbers $Pr < 0.1$. At the same time, these flows can be modelled experimentally by many transparent test fluids (e.g. water, silicon oils, salt melts), which have similar Prandtl numbers, but allow one to avoid the extremely high melting-point temperatures of the oxide materials. Most previous studies of melt instabilities for Prandtl numbers larger than unity suffer from a lack of accuracy that is caused by the use of coarse grids. Recent convergence studies made for a series of simplified problems and for a hydrodynamic model of Czochralski growth showed that for a second order finite volume method reliable stability results can be obtained on grids having at least 100 nodes in the shortest spatial direction. The obvious numerical difficulties call for an extensive benchmark exercise, which is proposed here on the basis of recently published experimental and numerical data, as well as some preliminary results of this study. The calculations presented are performed by two independent numerical approaches, which are based on second-order finite volume and finite element discretizations. We start our comparison from the steady states, whose parametric dependencies sometimes exhibit turning points and multiplicity. We then compare the critical temperature differences corresponding to the onset of instability, and finally compare calculated supercritical oscillatory states and phase plots.

© 2008 WILEY-VCH Verlag GmbH & Co. KGaA, Weinheim

1 Introduction

Melt flow instabilities arising during the Czochralski (CZ) growth of bulk oxide crystals can lead to serious problems. Sometimes the instabilities are so serious that the growth process must be stopped, which dramatically reduces the yield. These hydrodynamic instabilities cause morphological changes, for example spiral formation. Figure 1 shows several examples of spiral growth arising after the onset of symmetry breaking in an initially axisymmetric process.

The basic assumption of this study is that the spiral growth is caused by a three-dimensional axisymmetry-breaking instability in the system, which includes heat transfer in the melt and in the crystal, as well as melt flow in the crucible. It is clear also that in order to study possible instabilities of the whole system, the melt flow must necessarily be taken into account. This fact is supported by figure 2, where a change of the crystal rotation direction has caused a change of the direction of the grown spiral, that again indicates the macroscopic nature of the instability. Because of the complexity of the whole problem, we focus on studying the instabilities of a non-isothermal melt flow only, thus assuming that the melt flow is the main source of instability.

* Corresponding author: e-mail: nesoc@ikz-berlin.de

Oxide crystalline materials have very high melting temperatures (about 2000°C [1]) making an experimental study of their melt flows extremely difficult. On the other hand these melts are characterized by Prandtl numbers in the range $5 < Pr < 20$. This allows one to use various transparent fluids having similar Prandtl numbers, e.g. water, silicon oils, salt melts, as an experimental liquid and consequently the melt flow driven by buoyant convection, thermocapillarity and rotation can be mimicked experimentally (see, e.g., [5,9]). Computational modelling of these flows has been carried out by many authors, and has been reviewed in [4]. However, as was shown in [2-4], most of these studies suffer from a lack of numerical accuracy. The convergence studies performed for simplified models of convective and rotational flows [2,3], as well as for some Czochralski melt flow configurations [4] showed that in order to obtain convergence using a second-order numerical method one needs more than 100 grid points in the shortest spatial direction. Additionally, it is shown here that steady and oscillatory states of CZ melt flow exhibit multiplicity similar to that in simpler model flows in rectangular and cylindrical domains. We argue here that dealing with the problematic convergence observed for large-Prandtl-number Czochralski melt flows, complicated by the multiplicity phenomenon, makes it necessary to define a benchmark exercise for the performance of different numerical codes. It is mandatory also to base such a benchmark exercise on the existing experimental setup, so that the numerical results can be validated against experiments.



Fig. 1 From left to right: DyScO₃ crystal showing an extreme case of spiral growth, DyScO₃ crystal with later onset of spiral growth, SmScO₃ with very distinctive spiral growth, SmScO₃ crystal with later onset of spiral growth. (Online color at www.crt-journal.org)



Fig. 2 DyScO₃ crystals grown in opposite rotation directions. The formed spirals show opposite turns. (Online color at www.crt-journal.org)

In this study we formulated a test problem for a Czochralski melt flow based on the recent experiments of Schawbe, Sumathi and Wilke [5]. This problem was treated by two independent computational codes which incorporate two different numerical approaches. The Israeli group (A. Yu. Gelfgat, E. Kit, School of Mechanical Engineering, Faculty of Engineering, Tel-Aviv University, Israel) is using a code based on the second-order finite volume method, while the German group (N. Crnogorac, H. Wilke, Institute for Crystal Growth (IKZ) Berlin, Germany) uses a FEM code with quadratic polynomial interpolation for the velocities and temperature and linear interpolation for the pressure. We compare results of calculations of steady state

flows, their instabilities and supercritical oscillatory regimes. In the following we present the problem formulation and several preliminary results on the calculations of steady state flows, their stability, and supercritical oscillatory states. Then we propose a set of benchmark exercises for the code validation. Conclusions based on our preliminary results are summarised at the end of the paper.

2 Model problem and numerical methods

The problem under study is a so-called hydrodynamic model of CZ melt flow, which considers flow in a non-uniformly heated cylindrical crucible, driven by buoyancy convection, thermocapillary convection and rotation of the crystal. The detailed formulation and definitions are given in [4,6] and are briefly repeated here. The CZ melt flow is governed by the momentum, continuity and energy equations in the Boussinesq approximation. We consider a flow of melt with kinematic viscosity ν , density ρ and thermal diffusivity χ in a cylindrical crucible $0 \leq r \leq R_{crucible}$, $0 \leq z \leq H$ in cylindrical coordinates. To nondimensionalise the equations the scales $R_{crucible}$, $R_{crucible}^2/\nu$, $\nu/R_{crucible}$, $\rho(\nu R_{crucible})^2$ for length, time, velocity and pressure, respectively, are used. The temperature is nondimensionalised by the relation $T = (T^* - T_{cold}^*) / (T_{hot}^* - T_{cold}^*)$, where T_{hot}^* and T_{cold}^* are the maximal and minimal temperatures at the boundaries of the flow region. The set of equations for the non-dimensional velocity $\mathbf{v} = \{v_r, v_\theta, v_z\}$, temperature T and pressure p in the domain $0 \leq r \leq 1$, $0 \leq z \leq A$ reads

$$\frac{\partial \mathbf{v}}{\partial t} + (\mathbf{v} \cdot \nabla) \mathbf{v} = -\nabla p + \Delta \mathbf{v} + Gr \theta \mathbf{e}_z \quad (1)$$

$$\frac{\partial T}{\partial t} + (\mathbf{v} \cdot \nabla) T = \frac{1}{Pr} \Delta T, \quad \nabla \cdot \mathbf{v} = 0 \quad (2,3)$$

Here $A = H/R_{crucible}$ is the crucible aspect ratio, $Gr = g\beta(T_{hot}^* - T_{cold}^*)R_{crucible}^3/\nu^2$ the Grashof number, $Pr = \nu/\chi$ the Prandtl number, g the gravity acceleration, β the thermal expansion coefficient, and \mathbf{e}_z the unit vector in the z -direction. The velocity boundary conditions are

$$v_r = v_z = 0 \text{ at } z = 0, r = 1 \text{ and } z = A, \quad 0 \leq r \leq \eta, \quad \eta = R_{crystal}/R_{crucible}, \quad (4)$$

$$v_\theta = 0 \text{ at } z = 0 \text{ and } r = 1, \quad (5)$$

$$v_\theta = Re_{crystal} r \text{ at } z = A, \quad 0 \leq r \leq \eta, \quad (6)$$

$$v_z = 0, \quad \frac{\partial v_r}{\partial z} = -MaPr \frac{\partial T}{\partial r}, \quad \text{at } z = A, \quad \eta \leq r \leq 1. \quad (7)$$

Here $Ma = \gamma(T_{hot}^* - T_{cold}^*)R_{crucible}/\rho\nu^2$ is the Marangoni number, $Re_{crystal} = \Omega_{crystal}R_{crucible}^2/\nu$ is the crucible rotation Reynolds numbers, and γ is the coefficient of the assumed linear dependence of the surface tension coefficient on the temperature. The boundary conditions for the dimensionless temperature T are given by

$$T = 1 \text{ at the crucible sidewall; } T = 0 \text{ at the melt/crystal interface;} \quad (8)$$

$$T = 0.8571 + 0.1429 \left(\frac{r}{R_{crucible}} \right)^2 \text{ at the crucible bottom;} \quad (9)$$

$$\frac{\partial T}{\partial z} = -BiT \text{ at the free surface} \quad (10)$$

In the above formulation we choose $R_{crucible}$ as the characteristic length to make it easier to alter the crystal radius as was done in the recent experiments of Teitel, Schwabe and Gelfgat [9]. In eq. (10) we also assumed that the ambient temperature is equal to the temperature at the melt/crystal interface. This is apparently wrong for the realistic crystal growth, however it does correspond to the model experiments [5]. Defining $\Delta T = T_{hot} - T_{melting}$ and using the geometric and material data of [5] we estimate the governing parameters as $Pr=9.2$, height/radius=0.92, the crystal to crucible radii ratio 0.5, $Bi=0.1$, $Gr=1.90 \times 10^5 \Delta T$ and $Mn=MaPr=586 \Delta T$, where ΔT is measured in K. In the following we consider the dimensional temperature

difference ΔT as a critical parameter. This is a necessary choice since both Grashof and Marangoni numbers are affected by the value of ΔT . Moreover, ΔT and the crystal rotation rate are the only parameters that can be varied in the experiment.

Two independent numerical codes are applied. The finite element code of the German group is based on a discretization containing up to 200×200 non-uniform quadrilateral elements with biquadratic interpolation for the velocity and temperature fields and bilinear interpolation for the pressure. The finite volume code of the Israeli group is also of the second order and uses staggered and stretched grids with up to 1000×1000 nodes. Both codes include a direct calculation of steady flow states and time-dependent computations. The finite volume code contains also an eigenvalue solver, which allows us to study three-dimensional linear stability of axisymmetric steady states. The details can be found in [4,6].

3 Results and discussion

Steady state flows The study is started from a calculation of steady states that sometimes exhibit turning points and multiplicity. We then compare the critical temperature differences corresponding to the onset of instability, and finally the calculated supercritical oscillatory states and phase plots. Examples of calculated steady state flows are shown in figure 3 for $\Delta T=1.0\text{K}$ and the Reynolds number 0, 1000 and 5000. The solid lines in figure 3 are equally spaced between the maximum and minimum values. The maximum and minimum values of the temperature are 0 and 1, of the azimuthal velocity are 0 and Re , and those for the stream function are reported in table 1.

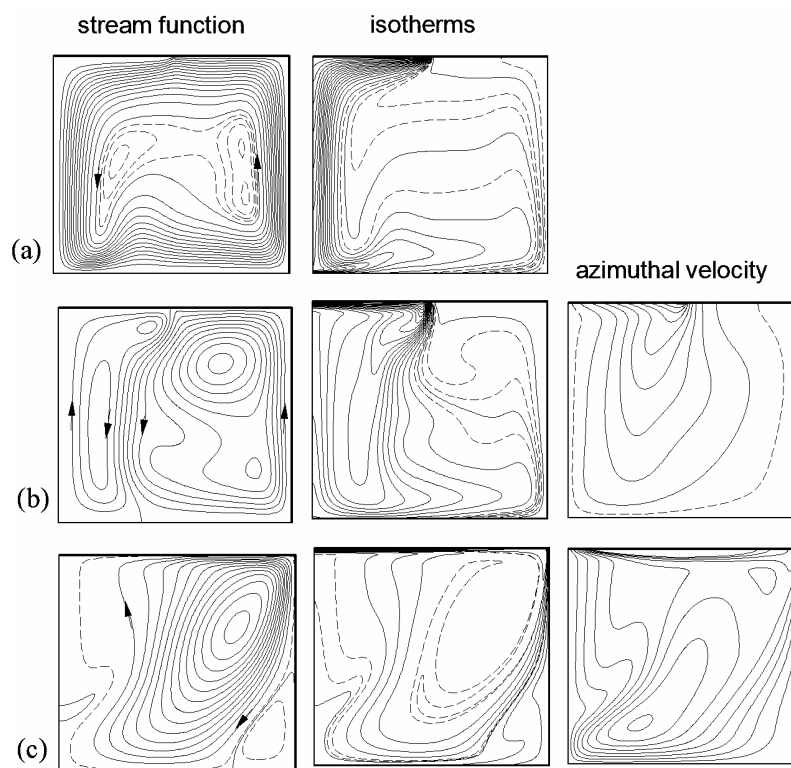


Fig. 3 Stream function (left frames), isotherms (middle frames), and isolines of azimuthal velocity calculated by the finite volume method on 200×200 stretched grid for $\Delta T=1$. (a) $Re=0$, (b) $Re=1000$, (c) $Re=5000$. Solid lines are equally spaced. Dash lines are added to illustrate more details of the patterns. The left border of each frame corresponds to the symmetry axis.

Table 1 contains some quantitative properties of the flows shown in figure 3, which can be used for a comparison. They are: maximum and minimum values of the stream function and their location $\psi_{min/max}(r,z)$; maximum and minimum values of the radial velocity at the cross-section $r=0.5$ and their locations $u_{min/max}(r=const.,z)$; maximum and minimum values of the axial velocity at the cross-section $z=0.5A$ and their locations $w_{min/max}(r,z=const.)$; total kinetic energy of the flow E_{kin} ; Nusselt numbers at the bottom Nu_{bottom} , side wall Nu_{wall} , crystal surface $Nu_{crystal}$, and free surface $Nu_{surface}$; leading eigenvalue of the problem linearized in the vicinity of the corresponding steady state. It is seen that results obtained by the two codes are reasonably

close, however, do not coincide even to within the second decimal digit. This indicates on the absence of a complete convergence, which affects the stability results shown below.

Table 1 Characteristic values for steady state flows at $\Delta T=1.0\text{K}$ and different Reynolds numbers.

Re	Finite volume code (Israeli group), stretched grid 200×200			Finite element code (German group), 120×120 biquadratic elements		
	0	1000	5000	0	1000	5000
$\Psi_{\min} / (r_{\min}, z_{\min})$	-1.510 / (0.8100, 0.3263)	-2.070 / (0.6900, 0.6797)	-1.206 / (0.8652, 0.1610)	-1.502 / (0.7904, 0.3246)	-2.130 / (0.6701, 0.6802)	-1.203 / (0.8696, 0.1597)
$\Psi_{\max} / (r_{\max}, z_{\max})$	0.0	0.7079 / (0.1770, 0.4600)	26.71 / (0.7500, 0.6087)	0.0	0.7102 / (0.1798, 0.4501)	24.85 / (0.7450, 0.6195)
$u_{\min}(r=0.5) / z_{\min}$	-36.55 / 0.9183	-33.94 / 0.9183	-145.8 / 0.05774	-36.61 / 0.9013	-33.10 / 0.9104	-146.3 / 0.0611
$u_{\max}(r=0.5) / z_{\max}$	14.63 / 0.08736	11.83 / 0.08736	475.5 / 0.9075	15.02 / 0.0842	11.88 / 0.0860	478.3 / 0.9092
$w_{\min}(z=0.5A) / r_{\min}$	-231.8 / 0.0	-35.52 / 0.2631	-157.5 / 0.8577	-232.2 / 0.0	-35.40 / 0.2603	-155.5 / 0.8595
$w_{\max}(z=0.5A) / r_{\max}$	15.76 / 0.9477	124.4 / 0.0	192.9 / 0.4039	15.78 / 0.9502	126.4 / 0.0	193.7 / 0.4014
E_{kin}	80.92	54.83	4262.	83.92	55.89	4280.1
Nu_{bottom}	1.575	1.499	0.7685	1.580	1.502	0.757
Nu_{wall}	1.246	1.185	7.306	1.231	1.155	7.352
Nu_{crystal}	-2.784	-2.647	-8.053	-2.785	-2.634	-8.093
Nu_{surface}	-0.036	-0.037	-0.0215	-0.026	-0.023	-0.016
Leading eigenvalue	(-0.06967, 0.1494)	(-0.005880, 0.05768)	(-0.25232, 0.1217)	not calculated	not calculated	not calculated

When the crystal is stationary ($Re=0$, Fig. 3a) the flow is driven by the buoyancy and thermocapillary forces, which create a counter-clockwise convective circulation. Note that this counter-clockwise motion would be created by each of the two forces separately, so that the two driving mechanisms enhance each other. This flow pattern is characterized by an intensive descending flow near the axis, where the temperature changes rapidly. This region is interpreted sometimes as a “cold jet” and is a source of the experimentally observed so-called “cold plumes” and “cold jet” instabilities [5,9]. We observe also the velocity boundary layer near the crucible wall. These two regions with rapid variation in the velocity and temperature make the calculations very demanding with respect to the numerical accuracy.

With the increase of crystal rotation we observe the increasing action of centrifugal force, which tends to create a circulation in the clockwise direction, opposite to the convective circulation (Fig. 3b). At $Re=1000$ this splits the main circulation into two: the clockwise one located below the crystal and driven mainly by the centrifugal force, and the counter-clockwise one located below the free surface and driven mainly by the buoyancy and thermocapillary forces. Note that in this case the total kinetic energy and the total heat transfer through the cavity are both reduced compared to the case of a non-rotating crystal (Table 1). Regions of a rapid variation in the velocity and temperature also disappear, which makes the numerical calculations less demanding. Really, it follows from table 1 that results obtained by two codes are closer at $Re=1000$ and 5000 than at $Re=0$. This seemingly surprising result is a sequence of a smearing of the boundary layer and the “cold jet” region by rotation.

At very large Reynolds number the centrifugal force is dominant and the circulation rotates clockwise (Fig. 3c). The flow pattern is similar to a so-called rotating disk – cylinder flow [10,11]. At large rotation rates we also observe a dramatic change in the shape of the isotherms caused by the strong effect of thermal convection. The total kinetic energy and the total heat transfer through the melt volume are dramatically increased. Obviously, this case should be considered as an extreme for the usual parameters of oxide crystal growth. However, it is important for understanding the stability properties of the flow, as well as being another representative case for numerical benchmarking. Note also that the boundary layers developing near the crucible wall (fig. 3c) again place greater demands on the computations.

The comparison of path-following techniques of [4,8] used for calculation of steady states is shown in fig. 4. The steady flows at $\Delta T = 0.27\text{K}$ and Reynolds numbers varied between 0 and 2000 where compared. The total kinetic energy of the flow was chosen to illustrate the parameter-dependence of the steady states and the comparison. The first observation of fig. 4 shows that the curves of German and Israeli groups are in very good agreement. For $Re < 1200$ and $Re > 1600$ we observe a single steady-state solution. In the interval $1200 \leq Re \leq 1600$ we observe two turning point bifurcations. Inside this interval the result is dependent on the initial conditions. Thus, for $Re=1375$ (shown by a vertical line in fig. 4) the first solution with the smallest kinetic energy is a stable steady state, the next one is unstable below the curve and is stable above it, and the third solution corresponds to a Hopf bifurcation point, i.e., onset of an oscillatory instability. The steady states at the third branch are stable at the right hand side of the curve and are unstable at the left hand side of it. Such instability can possibly lead to the spiral crystal formation. It should be noted that multiple solutions appear for

the values of Reynolds number characteristic for real crystal growth process. For example, $Re=1375$ corresponds to the crystal rotation with the angular velocity of approximately 12 rpm. It should also be mentioned that the value of $\Delta T = 0.27\text{K}$ is much smaller than that applied in the oxide crystal growth equipment. Finally, it is stressed that the existence of multiple steady states and the dependence of the final state on the initial conditions is well-known for model convection and rotating flow. Several examples can be found in the review paper [12]. To the best of our knowledge, the multiplicity of steady state flows has not previously been reported for the CZ configuration.

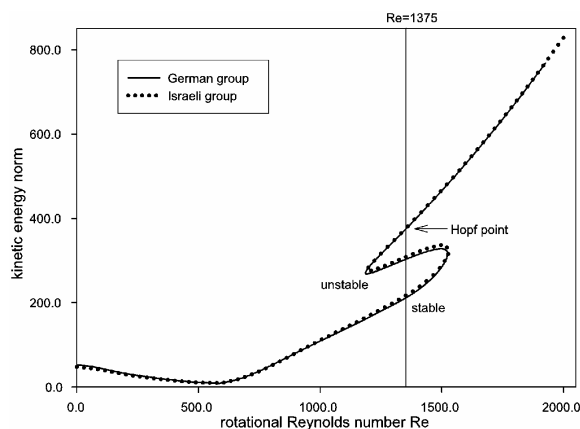


Fig. 4 Continuation diagram for control parameter Re for $\Delta T=0.27\text{K}$.

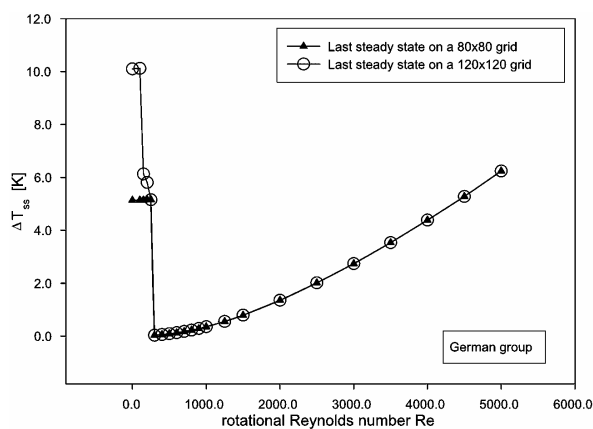


Fig. 5 Stability diagrams of NaNO_3 -melt flow in a CZ-crucible using a 80×80 FEM grid and a 120×120 FEM grid, respectively.

Figure 5 shows an example of the grid-dependence study. With the help of direct numerical simulation (DNS starts from an initial guess in order to obtain a steady state or time-dependent solution.), which is very time consuming, we have calculated step by step two stability diagrams of the melt flow in a CZ crucible for two different FEM grids. Every point on the curves in figure 5 shows the last converged steady state solution for a certain parameter combination on a given grid. We can see that for small rotational Reynolds numbers the numerical simulations of this kind are strongly grid dependent. Apparently, this is the effect of steep velocity and temperature change near the crucible axis and the boundary layer close near the crucible wall. To retain the numerical accuracy we have to use a finer grid at small rotational Reynolds numbers. As mentioned above, calculations for larger Reynolds numbers converge at coarser grids because the boundary layers smear due to the action of the centrifugal force.

Stability limits and unsteady flows Neutral stability curves corresponding to the oscillatory instability of steady state flows with respect to the axisymmetric perturbations are shown in figure 6. Preliminary results corresponding to the three-dimensional perturbations can be found in [4]. Here we focus mainly on the comparison exercise, which we start from the axisymmetric instability. The stability diagram in figure 6 shows the critical temperature difference ΔT_{cr} for different rotational Reynolds numbers. Below the stability curve the melt flow is linearly stable and is unstable above the curve. The solid and dashed curves in figure 7 show results of the stability study carried out by the German and Israeli groups, respectively. The curves are plotted through calculated Hopf bifurcation points in which the leading eigenvalues of the linearized stability problem appear as conjugate complex pairs having zero real parts. Hopf bifurcation points are origins of oscillatory solution branches (periodic orbits).

For rotational Reynolds numbers $Re > 400$ the results of both groups are in good agreement (Fig. 6). For small rotational Reynolds numbers $Re < 400$ the results of the two groups disagree. Reasons for this disagreement are not completely clear yet. Here we stress again that calculations at zero and small Reynolds numbers are more difficult, which is also reflected in the current disagreement. Possible reasons for the disagreement are grid dependence of different numerical approaches (FVM vs. FEM) or overlooking of the most dangerous eigenvalues. The last possibility always exists in such computations, since only a part of the spectrum is computed [4]. At the same time the good agreement obtained for $Re > 400$ is important since these Reynolds numbers are close to the real oxide crystal growth conditions, where crystal rotation rates vary between 5 and 25 rpm ($Re=5000$ corresponds to 50 rpm).

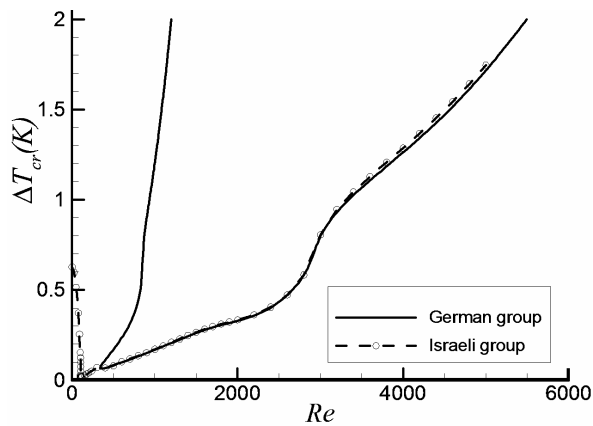


Fig. 6 Stability curves for the critical temperature difference versus Reynolds number.

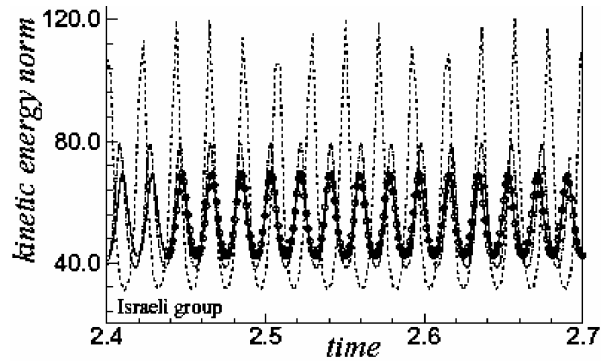


Fig. 7 Time history of the kinetic energy norm of the flow for rotational Reynolds number $Re=0$ and $\Delta T=0.6K$ calculated with different time steps on the grid 100×100 by the finite volume method. (dashed line - $\Delta t=0.1$, dash-and-dot line - $\Delta t=0.01$, solid line - $\Delta t=0.001$, symbols - $\Delta t=0.0001$).

In carrying out time-dependent calculations one has to also consider the time-step dependence. Figure 7 illustrates a possible effect of a too large time step. It is seen that a too large time step leads to a time-asymptotic periodic solution that overestimates the oscillation amplitude and also affects its period. At the same time such a simple comparison allows us to conclude that there is no visible difference between the two smallest time steps used. The results obtained agree well with the oscillation period yielded by the linear stability analysis. We must also be aware that with the increase of ΔT or Re it will be necessary to reduce the time step further, and at some stage to repeat the convergence study. This example shows that time-dependent calculations done without a proper examination of the time-step dependence may lead to misleading conclusions.

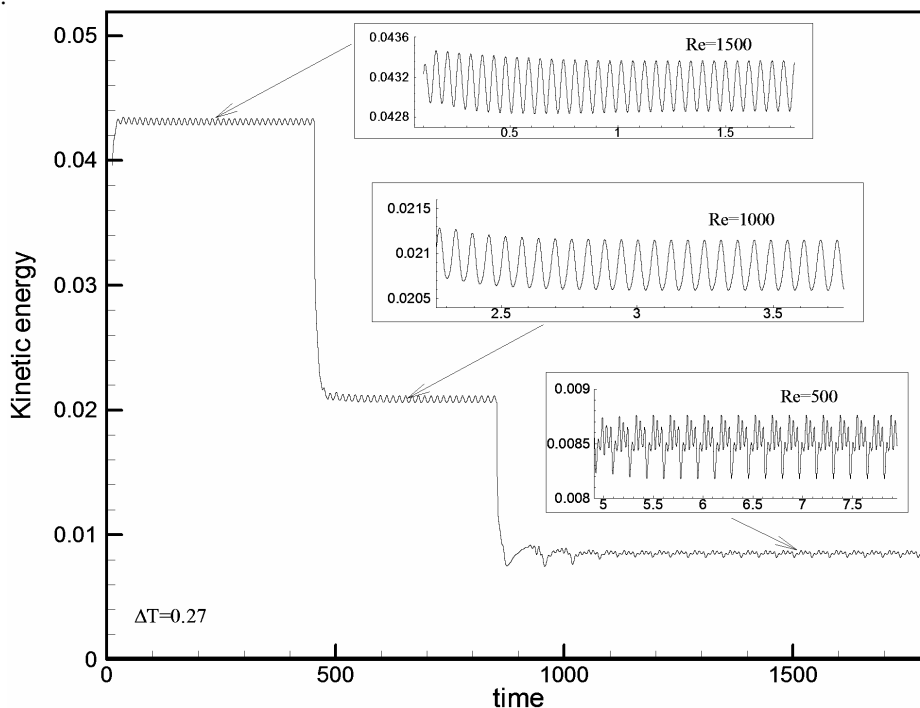


Fig. 8 Transient simulations for different rotational Reynolds numbers for constant $\Delta T=0.27K$. Calculation by the finite volume method on 100×100 grid.

According to the stability diagram shown in figure 6 the flow at $\Delta T=0.27\text{K}$ and $Re=1500$ is oscillatory and remains oscillatory unstable at $Re=1000$. At $Re=500$ the steady state is oscillatory and unstable according to results of Israeli group (dash line in fig. 6), but is stable due to results of German group (solid line in fig. 6). This issue was investigated by time-dependent calculations, which started from oscillatory unstable state at $Re=1500$, and then the Reynolds number was abruptly reduced to the values of 1000 and 500. The results are shown in figures 8 and 9.

Figure 8 shows the result of time-dependent calculations carried out by Israeli group. For $Re=1500$ and $\Delta T=0.27\text{K}$ the oscillations become sinusoidal after a certain period of time. With the decrease of the Reynolds number to 1000 we still observe sinusoidal oscillations. In spite of the visible decrease in the total kinetic energy, the amplitude of oscillations remains almost unchanged. Further decrease in the Reynolds number to the value of 500 again leads to a decrease in the total kinetic energy.

To compare time-dependent results we use phase plots that show change in the temperature and the axial velocity at the point $r=0.13$, $z=0.8$ over several oscillation periods (Fig. 9). The phase plots calculated by both groups with the established time-step convergence coincide for $Re=1000$, and agree only qualitatively for $Re=500$ and 1500. It shows again that the grid-dependence issue should be carefully checked when governing parameters are varied in large intervals. Another interesting observation is the oscillatory state at $Re=500$ obtained by German group which is in apparent conflict with the prediction of their stability diagram shown in figure 6. However, as shown in [6], this happens because of the simultaneous existence of stable steady state along with the oscillatory one.

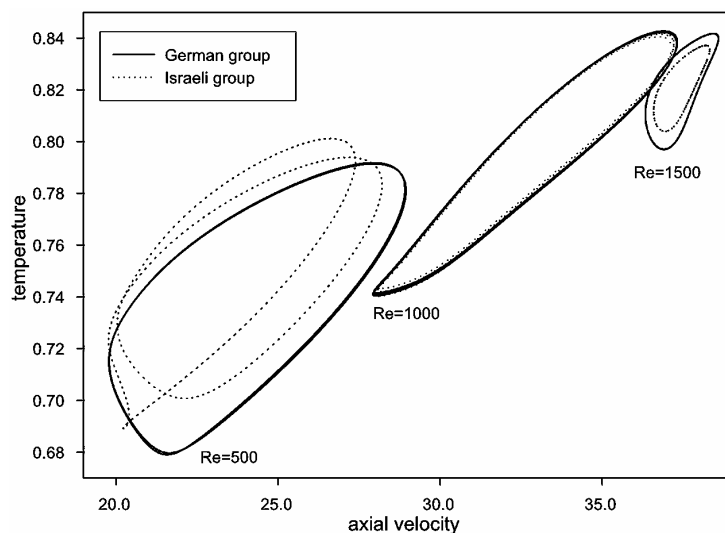


Fig. 9 Phase plots for different rotational Reynolds numbers at a position close to the solid liquid interface for $\Delta T=0.27\text{K}$.

4 Suggestion of a benchmark exercise

The above results show the importance of the choice of the grid size and the time step for obtaining reliable results for computational modelling of melt flow in Czochralski growth of oxides and other large-Prandtl-number materials. On the basis of these calculations, we propose a benchmark exercise that comprises three separate sets of comparisons related to calculation of steady states, analysis of their stability and calculation of supercritical oscillatory states. Taking the present problem formulation and values of A and Pr , and the dependence of Ma and Gr as given in section 2, the benchmark problems are defined as follows.

Set 1: calculation of steady states

- 1 to report data of table 1 (except the eigenvalue) for $\Delta T=1\text{K}$ and $Re = 0, 500, 1000$, and 1500
- 2 to calculate the parameter-continuation diagram of figure 4. The purpose of this task is to validate the calculation of steady states and to establish the evidence of the existence of multiple steady states in the CZ melt flow.

Set 2: stability analysis

- 1 To calculate leading eigenvalues corresponding to the axisymmetric perturbations for $\Delta T=1\text{K}$ and $Re = 0, 500, 1000$, and 1500.

- 2 To calculate marginal stability curve as shown in fig. 6 for axisymmetric instability of the flow.
- 3 For the parameters of 2(i) consider three-dimensional perturbations and calculate leading eigenvalues for the azimuthal wavenumbers varying from 1 to 5 (for details see [4]).
- 4 To calculate marginal stability curves as shown in fig. 6 for three-dimensional instability of the flow for the azimuthal wavenumbers varying from 1 to 5.

Set 3: time-dependent calculations

- 1 For $\Delta T=0.27K$ to perform unsteady time-dependent axisymmetric calculations with an abrupt increase of the Reynolds number from $Re=50$ to $Re=100, 200, 300, 500, 1000,$ and 1500 . Report the asymptotic steady or oscillatory state as a time history of the total kinetic energy.
- 2 Repeat 3(i), but starting from the asymptotic state at $Re=1500$ and abruptly reducing the Reynolds number to $Re=1000, 500, 300, 100$ and 50 . This exercise is aimed to check a possible existence of hysteresis phenomenon. In this way we can show that there exist simultaneously several oscillatory states or a steady and an oscillatory state.
- 3 To perform fully 3D calculations for $\Delta T=0.7K$ and $Re=0$, and for $\Delta T=0.15K$ and $Re=1000$. Note, that these parameters are based on the results of [4], which yet to be validated.

Note that the tasks of this benchmark partially repeat the tasks of three well-known benchmarks of convection flows in rectangular cavities [13-15], which dealt with steady states [13], oscillatory instability [14], and slightly supercritical oscillatory flows [15]. The benchmark quality data for a rotating disk – cylinder flow is also established. The benchmark proposed here considers much more complicated flow, which, according to our numerical experience, is much more demanding with respect to the required numerical accuracy. Additionally, it is directly related to the CZ growth of oxide crystals and may be interesting to a wide community of researchers that do not deal with numerical methods and use commercial codes for their research needs.

5 Concluding remarks

Steady states, their stability and slightly supercritical oscillatory states of a model of CZ melt flow were studied numerically by two independent numerical approaches. It has been argued that spiral instabilities observed in the growth of rare-earth scandates are caused by instabilities in the melt flows. The set of computations reported here shows how the flow patterns change with the increase of crystal rotation rate, at which parameters the oscillatory instability of the flow sets in and how it develops at slightly supercritical parameters. The existence of multiple steady and oscillatory flow states means that for a transient CZ growth the final asymptotic flow state depends on the initial conditions, i.e. on the history of the process. This is in agreement with the previous observations made for simplified flow models [12] and should be taken into account in the research and development of CZ crystal growth processes.

We showed here that computational modelling of large-Prandtl-number CZ melt flows is extremely demanding with regard to numerical accuracy. The two numerical approaches applied here showed good agreement in most of the comparisons done. However, there is some disagreement that has to be resolved in our future studies or by comparison with other independent studies. For the latter purpose we propose here a benchmark exercise that includes comparisons for steady and oscillatory flows, as well as for the stability results that partially disagree.

Acknowledgements This work was supported by the German-Israeli Foundation, Grant no. I-794-145.10/2003. The German group also thanks the Norddeutscher Verbund für Hoch- und Höchstleistungsrechnen (HLRN) for providing HPC facilities and support.

References

- [1] R. Uecker, H. Wilke, D. G. Schlom, B. Velickov, P. Reiche, A. Polity, M. Bernhagen, and M. Rossberg, *J. Cryst. Growth* **295**, 84 (2006).
- [2] A. Yu. Gelfgat, *Int. J. Numer. Meths. Fluids* **53**, 485 (2007).
- [3] A. Yu. Gelfgat, *Int. J. Numer. Meths. Fluids* **54**, 269 (2007).
- [4] A. Yu. Gelfgat, in: "Studies on Flow Instabilities in Bulk Crystal Growth" (ed. A. Gelfgat), Transworld Research Network, 2007.

- [5] D. Schwabe, R. R. Sumathi, and H. Wilke, *J. Cryst. Growth* **265**, 440 (2004).
- [6] H. Wilke, N. Crnogorac, and K. A. Cliffe, *J. Cryst. Growth* **303**, 246 (2007).
- [7] A. Yu. Gelfgat, A. Rubinov, P. Z. Bar-Yoseph, and A. Solan, *J. Cryst. Growth* **275**, e7 (2005).
- [8] K. A. Cliffe, A. Spence, and S. J. Tavener, *Acta Numerica* **39** (2000).
- [9] M. Teitel, D. Schwabe, and A. Yu. Gelfgat, *J. Cryst. Growth* (to appear).
- [10] A. Yu. Gelfgat, P. Z. Bar-Yoseph, and A. Solan, *J. Fluid Mech.* **311**, 1 (1996).
- [11] A. Yu. Gelfgat, P. Z. Bar-Yoseph, and A. Solan, *J. Fluid Mech.* **438**, 363 (2001).
- [12] A. Yu. Gelfgat and P. Z. Bar-Yoseph, *Int. J. Numer. Meth. Heat Fluid Flow* **14**, 213 (2004).
- [13] G. de Vahl Davis and I. P. Jones, *Int. J. Numer. Meth. Fluids* **3**, 227 (1983).
- [14] B. Roux (ed.), "Notes on Numerical Fluid Mechanics", 1990, p. 27.
- [15] M. A. Christon, P. M. Gresho, and S. B. Sutton, *Int. J. Numer. Meth. Fluids* **40**, 953 (2002).